Desalination and Water Treatment
www.deswater.com
doi: 10.5004/dwt.2023.29596

295 (2023) 227–244
May

High adsorptive removal of cationic dye using carboxylated and mechanically attrited activated carbon

Haradip Kumar Mahilary, Amit Kumar Dey*

Department of Civil Engineering, Central Institute of Technology Kokrajhar, Assam, India-783370, email: ak.dey@cit.ac.in (A.K. Dey)
Orchid ID: 0000000340700231

Received 17 September 2022; Accepted 27 April 2023

ABSTRACT

Malachite green (MG), a cationic dye, is evaluated for removal using carboxylated activated carbon that was made using an organochlorine chemical and sodium hydroxide in a wet milling process (MCGT-AC). Utilizing research in Brunauer–Emmett–Teller (BET), X-ray diffraction, environmental scanning electron microscopy, energy-dispersive X-ray spectroscopy, Fourier-transform infrared spectroscopy, and high-resolution transmission electron microscopy, adsorption processes were described. As per zeta potential and point of zero charge analysis a suitable and stable pH of 6.5 was considered for the modelled dye solution with increasing pH supporting the sorption process well. It just took 30 min for the MG dye to reach equilibrium with the MCGT-AC. The experimental findings agree well with the Langmuir isotherm, which has a maximum adsorption capacity of 251.6 mg/g, according to isotherm study and error analysis. The activation energy (E_a = 51.36 kJ/mol) indicated that chemisorption was responsible for controlling the process. BET study showed that the sorbent's post-process pore size dramatically decreased, supporting effective adsorption. Overall, adding functional groups (carboxyl, hydroxyl, etc.) to the modified adsorbent surface improved the sorption capacity of MCGT-AC with activated carbon that had been surface modified with carboxylic groups. The initial dye concentration, adsorbent dose, contact time, pH, and other operational parameters were examined. Regeneration research on utilized MCGT-AC revealed that during the sixth cycle, adsorption capacity dropped from 95.7% to 48.6%. According to the results, MCGT-AC may be used as a cost-effective and effective adsorbent for the treatment of industrial wastewater, including dyes.

Keywords: Mechanical attrition; Adsorption; Carboxylic group; Regeneration; Desorption; Activation energy

1. Introduction

Malachite green (MG), an organic cationic dye [chemical formula: $C_{23}H_{25}ClN_2$ (chloride)], is used to colour paper as well as dye cottons, wools, silk, leather, and paper stock coating. Despite MG's well-documented antiseptic, antibacterial, and anti-protozoan qualities, oral consumption of MG has been linked to cancer, mutagenesis, chromosomal fractures, teratogenicity, and respiratory toxicity [1–4]. When malachite green meets the skin or eyes, it causes irritation, redness, and pain [5]. The treatment of effluents containing such colours is of great interest because of the deleterious impact on receiving water [6]. Reverse osmosis, flocculation, biological degradation, nanofiltration, photocatalytic degradation, adsorption, ozonation, chemical oxidation and electrochemical degradation are some of the most frequently used techniques for removing different colours from aqueous solutions and industrial wastewaters [7,8]. Despite these tried-and-true strategies, efforts to find ways that are acceptable and have high efficacy, low cost, and ease of implementation remain uncommon [9]. The adsorption technique is thought to be better to other

* Corresponding author.

dye wastewater treatment technologies because it is more cost-effective, inert to dangerous chemicals, simple to operate, and has a higher dye removal capability [10]. The regeneration and efficiency of the adsorbents impact the cost of dye removal using the adsorption technique. When eliminating organic colour pollutants from wastewater, activated carbon (AC), which is made from a variety of materials, is used as an adsorbent [7,9,11,12]. This widespread use of AC can be explained by its highly porous structure, which has a well-oriented surface area and an affinity for adsorbates [13]. Different activation techniques are being used to activate the carbon generated from waste biomaterials while AC is being used with multiple types of pollutants [14]. The most expensive step in the AC preparation process is the activation. Several compounds are used to alter and activate the carbon surface in order to increase the organic dye's ability to adsorb substances [15]. Comparing NaOH activation to carbon activation with other chemicals, NaOH activation is less costly and less harmful to the environment. Because of surface interactions, NaOH is an appropriate activating agent for randomly oriented carbon composites [16]. In one study, cationic dyes were removed from water using an AC/$CoFe_2O_4$ magnetic composite, which had adsorption capacities of 86.24, 83.90, and 87.48 mg/g for methylene blue, methyl violet, and nile blue, respectively [17]. Because of their hollow layered structures, large specific surface areas, and potent electrostatic interactions, carbon nanomaterials (CNMs) have also received a lot of attention in the wastewater treatment field [18–20]. Despite their benefits, CNMs have a number of drawbacks, including hydrophobicity, poor aqueous dispersibility, and non-reactive surfaces, which would be counterproductive if utilised as an adsorbent [21,22]. By adding several functional groups to the surface of CNMs, which can occasionally be a complicated process, surface modification is expected to improve the surface characteristics of CNMs. On the other hand, surface-modified AC may produce crystalline carbon that is very mesoporous and has high dye sorption properties in aqueous conditions [23]. According to a paper [23], wet milling may be used to successfully activate carbon. When compared to raw carbon, milled carbon exhibited a much greater adsorption capacity. By enabling rapid mass transfer and the creation of new active sites during the activation phase of activated carbon, the milling technique improves efficiency and lowers dye adsorption costs [23].

In the current analysis, activated carbon (AC) was made from water hyacinth. Next, the surface of the adsorbent was simultaneously treated with carboxylic groups using NaOH and an organochlorine compound (chloroacetic acid ($C_2H_3ClO_2$)) using a wet milling process (mechanical attrition), to increase the potential for dye removal. To characterise the generated material, Brunauer–Emmett–Teller (BET), X-ray diffraction (XRD), environmental scanning electron microscopy (ESEM), energy-dispersive X-ray spectroscopy (XEDS), high-resolution transmission electron microscopy (HR-TEM), Fourier-transform infrared spectroscopy (FTIR), and zeta potential tests were carried out. Cationic dye MG was used as an adsorbate to evaluate the performance of milled and carboxylic group treated AC (MCGT-AC) as an adsorbent. Work using milled and carboxylated AC as an adsorbent is not reported much for sorption of cationic dyes.

2. Materials and methods

2.1. Chemicals and other material for AC preparation

Malachite green (MG), locally sourced water hyacinth (for making AC), NaOH, and an organochlorine compound ($C_2H_3ClO_2$) were among the analar grade compounds taken into consideration. HiMedia India provided all the chemicals and reagents, and they were all 99.9% pure. Fig. 1 depicts the molecular structure of the MG dye, which has a molecular weight of 364.911 g/mol and the chemical formula $C_{23}H_{25}ClN_2$ (chloride).

2.2. Carbon from water hyacinth

From Kokrajhar, Assam, India, water hyacinth samples were obtained from nearby water bodies and properly cleaned. The plant material was then cut into smaller pieces, the roots being removed, and sun-dried for two weeks in a nursery facility. The dry materials were cut into slices with a width of less than 0.5 cm and a length of less than 1 cm to prepare them for carbonization [24]. Water hyacinth was carbonized using the pyrolysis process [25]. A carbonization method was performed on water hyacinth for 60 min at 500°C to produce water hyacinth carbon (WH-C). Additionally, a 1:3 NaOH (in weight proportion) in an activator (make: Merck KGaA, Darmstadt, Germany) was used to chemically activate the carbon made from water hyacinth. On a magnetic stirrer hot plate at 80°C and 300 rpm, the WH-C was heated and swirled for 4 h. WH-C was then repeatedly washed with 0.1 M HCl and then distilled water. Additionally, the WH-C is dried until the mass is consistent in a 100°C oven [25]. The surface temperature of the carbonizer was measured using a thermocouple (DIGI-SENSE Model 20250-19). Average extraction rates of carbonized materials were 43.61 g/min (436.1 g in 10 min). As soon as possible, they were removed from the carbonizer and put in a covered desiccated glass container to cool and stop the carbon from generating ash [24]. Hereafter, "activated carbon prepared from water hyacinth (WH-AC)" refers to the prepared carbon.

2.3. Synthesis of milled and carboxylated AC

The procedure for converting WH-AC into MCGT-AC is as follows: A lab-scale ball mill facility (Make: Retsch, Model: planetary ball mill PM 100) was used to grind 5 g of WH-AC in a 250 mL grinding jar along with 50 mL of distilled water with 25 g of NaOH. The mill was operated for 6 h at a speed of 400 rpm, resulting in the formation of oxide groups on the AC surface. To create carboxylic groups on the

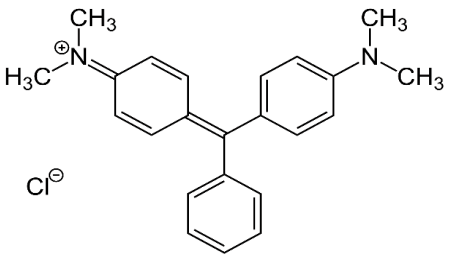

Fig. 1. Molecular structure of Malachite green.

AC surface, the mixture was then mixed with 25 g of chloroacetic acid and the mill was operated for additional 6 h at the same speed. The manufactured MCGT-AC was stored in a desiccated glass container for later usage after the product was adequately rinsed with distilled water and dried at 100°C for 24 h using a centrifuge [26].

2.4. Characterization studies

BET analysis is used to determine the pore volume, surface area, and pore-size distribution of MCGT-AC with an automated adsorption–desorption system (BELSORP-mini II, BEL Japan Inc.), based on N_2 adsorption data at –196°C. To ascertain the structure of the underlying crystal of the adsorbent, the nature of XRD was assessed using an X-ray diffractometer apparatus (Make: Shimadzu-Japan, Model: X-ray 6100) with the following specifications: Cu, K radiation = 0.1540 and a K filter at 30 mA, 30 kV. To attain the Bragg angle (2θ), a range of 5°–90° with a scanning rate of 5°/min was maintained. ESEM was used to examine the surface morphology of the adsorbent (Make: FEI, Model: Quanta 200, Specification: 3 nm resolution at 30 kV, ESEM mode), along with energy-dispersive X-ray spectroscopy for elemental analysis (XEDS). The samples were coated with gold using a sputtering coater (Model: S150B, Edwards High Vacuum Ltd., England) in order to prevent the development of local electrical charges during the XEDS analysis. FTIR was carried out using a device made by Bruker, Germany, model 3000 Hyperion microscope with vertex 80 FTIR system and array for focal plane 128 × 128, range 900–4,000 cm^{-1}, to identify the functional groups in charge of sorption. HR-TEM study (Make: JEOL, Model: JEM 2100F @ 200 kV) was done and analysed to investigate pore size and the development of adsorption layers. Zeta potential and point of zero charge (pH_{PZC}) study was carried out to ascertain the appropriate pH value for a stable solution for the sorption process and to assess the net surface charge of the adsorbent (MCGT-AC).

2.5. Batch analysis for dye adsorption

A stock solution of 1 g/L concentration for a 1,000 mL solution was first made from which solutions of various dye concentrations with various volumes were generated as needed. The adsorption trials employed the batch adsorption method. We investigated the effects of contact time (0–120 min), initial dye concentration (25, 50, and 75 mg/L), adsorbent (MCGT-AC) dose (10–50 mg), pH range (2–9), and temperature (298, 308, and 318 K). Finally, 1 mL of the suspension was extracted using a centrifugal method. The maximum absorbance wavelength range for MG dye is 579–624 nm, hence MG absorbance values at λ_{max} = 617 nm were determined using a UV-Visible spectrophotometer (Model: PerkinElmer Lambda 45), and then concentrations were measured. Eqs. (1) and (2) were used to calculate the dye adsorption capacity and removal percentage of adsorbed MG using the mass balance approach.

$$Q_e = \frac{C_0 - C_e}{m} V \tag{1}$$

$$\%\text{Removal of MG dye} = \frac{C_0 - C_e}{C_0} \times 100 \tag{2}$$

where starting and equilibrium dye concentrations are denoted by C_0 and C_e, respectively. The letters Q_e stand for adsorption capacity at equilibrium state in (mg/g), V for litres of MG dye solution, and m for grammes of MCGT-AC.

2.6. Point of zero charge and zeta potential

The point of zero charge is the pH at which an adsorbent surface has a net neutral charge (pH_{PZC}). Any adsorbent's ability to draw in cationic or anionic adsorbates may be determined by studying the pH_{PZC} for that adsorbent. The adsorbent surface will absorb anionic adsorbates when a solution with a pH lower than pH_{PZC} has a positive charge [27]. On the other hand, the adsorbent will absorb cationic adsorbate if the surface of the adsorbent has a negative charge in a solution with a pH higher than pH_{PZC} [28]. To determine the MCGT-AC's zero point of charge, seven flasks holding 50 mL of distilled water were set at various beginning pH values (pH_i) ranging from 2–9. 50 mg of MCGT-AC was added to each flask, which was then shaken for 24 h. To determine the final pH values (pH_f) of the aqueous solutions, adsorbent material was taken out of the mixture of solutions. The pH difference was calculated using the formula ($\Delta pH = pH_i - pH_f$). To determine the pH_{PZC} sign change point, pH values were plotted against pH values. Zeta potential and zero point of charge differ primarily in that the former refers to the potential difference between a dispersed MCGT-AC fluid's static layer and the surrounding medium, whereas the latter refers to the pH level of the dispersed MCGT-AC when the surface of the MCGT-AC bears net zero charge.

3. Results and discussions

3.1. Characterization studies

The adsorbent's volume of pores, surface area, and average pore radius sizes were calculated using BET analysis. The surface area of 25 mg of adsorbent that was heated to 300°C for 3 h was calculated. The procedure was completed in around 24 h. The principal pore-size distribution of the adsorbent was done on the pore-size distribution curve created by the Barrett–Joyner–Halenda (BJH) analysis, and the complete adsorption and desorption data are presented in Tables 1 and 2. A typical I type isotherm was discovered by adsorption and desorption phenomena. Prior to and following adsorption, the adsorbent surface area was 192.67 and 205.76 m^2/g, respectively. The multipoint BET was used to calculate the surface area in the 0.05–0.95 p/p_0 range. It confirms that when MG dye is adsorbed, the surface area of the adsorbent increases, demonstrating a clear reduction in the size of the pores produced by the accumulation of MG dye in the adsorbent's pores. Increased surface area favours this structural modification that takes place during the adsorption process [29]. The fact that most of the pores fall within the range of less than 30 nm shows that MCGT-AC is mesoporous, with ultrafine pore sizes and a sizable specific surface area.

The XRD patterns of MCGT-AC, before adsorption exhibits up to 16 separate wide peaks at different 2θ values (28.7°, 38.2°, 40.1°, 42.7°, 44.3°, 44.3°, 47.5°, 55.3°, 57.6°, 61.4°, 67.1°, 72.4°, 73.8°, 80.3°, 84.9°, and 88.4°), which are caused by the

Table 1
Brunauer–Emmett–Teller analysis parameters

Parameters	Adsorbent (MCGT-AC)	
	Before adsorption	After adsorption
Surface area (m^2/g)	192.67	205.76
Pore volume (cm^3/g)	29.67	21.54
Average pore size (nm)	27.89	19.34

Table 2
BJH analysis parameters

Parameters	Operation	Adsorbent (MCGT-AC)	
		Before adsorption	After adsorption
BJH pore volume (cc/g)	*A*	0.197	18.652
	D	29.344	19.653
BJH pore radius (Å)	*A*	19.562	23.655
	D	338.211	298.435
BJH surface area (m^2/g)	*A*	103.459	102.866
	D	1,798.433	1,399.324

inclusion of higher ion exchange sites indicating high crystalline structure of MCGT-AC after carboxylic treatment. After dye adsorption, peaks significantly shifted, shrank, and disappeared, which supported the MG adsorption. As opposed to 16 such crystalline peaks prior to adsorption, there were 9 peaks remaining after adsorption at varied 2θ values (35.4°, 39.6°, 41.7°, 45.8°, 53.3°, 69.9°, 77.1°, 81.7°, and 84.8°). While the peak's shifting following adsorption suggests that the unit cell is contracting because of the MG dye molecules occupying the sorbent surface, the disappearance and decrease in peak intensity and number suggest that the adsorbent structure is losing crystallinity because of dye adsorption.

A research using ESEM was done to look at the shape of the adsorbent surface. The surface morphological characteristics of untreated WH-AC showed the relatively smooth surface. After treatment and milling with carboxylic groups, the surface of MCGT-AC presented with a lot of undulations and unevenness on the surface, hinting at the development of significant number of pores/ionized sites available for adsorption. This resulted from the electrostatic interaction and adhesion of carboxylic molecules. After milling and adding a carboxylic group to the surface, a significant number of pores formed, supplying more effective ion exchange sites for adsorption. Morphological properties of dye adsorbed adsorbent revealed that MG dye particles adhered to and/or filled the pores of MCGT-AC, resulting in a reduction in pore size as a result of dye molecule adsorption. Overall, the results of the ESEM analysis showed that carboxylic group treatment combined with milling on activated carbon results in an activated morphological structure with a high number of active sites on the surface of the adsorbent and, ultimately, a high dye removal capacity by MCGT-AC [30]. Similarly, XEDS analysis is used to explore the element presence on WH-AC, MCGT-AC, and MG loaded MCGT-AC. Use of XEDS analysis to investigate the presence of elements on surfaces, revealed that C, Na, and O elements make up WH-AC, which is made using NaOH. After being subjected to the wet attrition process and treated with carboxylic groups, the MCGT-AC surface had extra Cu components. Afterwards, for MG adsorbed MCGT-AC, Na elements in MCGT-AC are replaced by Rb and Hg elements as a result of adsorption, but not in the same proportion. This confirms dye adsorption and creates composites with the adsorbent surface. As a result, MG sorption led to the formation of MCGT-AC-MG composites, confirming MG adsorption onto MCGT-AC. Similar sorption process for cationic dye has been reported earlier [24].

FTIR analysis was carried out to identify the several functional groups in charge of the MG adsorption process. Functional groups can be identified and characterised using FTIR. At the research centre SAIF Bombay in India, routine spectrum analysis was carried out. Figs. 2a and b display the MCGT-AC FTIR spectra before and after MG dye adsorption. The strong and broad band for MCGT-AC was detected at 3,451.38 cm^{-1}, as shown in Fig. 2a, because of the linked amine and hydroxyl groups. As a result of the existence of –CH asymmetric stretching, a value of 2,919.40 cm^{-1} was obtained. A peak of 1,630.46 cm^{-1} was ascribed to the carboxyl group's stretching vibration. The bands at 1,611.82 and 1,382.86 cm^{-1}, respectively, were given symmetric and asymmetric stretching vibrations of C=O groups.

The band at 1,216.87 cm^{-1} illustrates the C–O stretching of alcohols and carboxylic acids. Fig. 2b illustrates how after adsorption, the hydroxyl groups' symmetrical expanding vibration bands were moved from 3,451.38 to 3,429.21 cm^{-1}. The stretching band of carboxyl groups was changed from 1,630.46 to 1,709.40 cm^{-1}. After dye adsorption, peaks at the stretching bands of 1,611.82 and 1,382.86 cm^{-1} vanished, and new band peaks were found at 1,611.96 and 1,358.49 cm^{-1}. The peak for C–O also decreased, moving from 1,216.87 to 1,100.55 cm^{-1}. The analysis of the FTIR spectra revealed the disappearance and shifting of peaks at various frequencies. In addition, important bands experienced a increase in intensity following dye adsorption (the carboxyl group increased from 1,630.46 to 1,709.40 cm^{-1} and the hydroxyl group decreased from 3,451.38 to 3,429.212 cm^{-1}), which was caused by the dye molecules occupying the active pores, indicating successful MG adsorption.

The HR-TEM study confirmed the adsorption of dye molecules on the MCGT-AC surface and was used to measure the pore size, report magnified sorbent surface, and confirm the accumulation of adsorbate layer formation over the adsorbent. HR-TEM analysis illustrated how surface modification has resulted in a significant number of pores, which has allowed for the production of ultra-fine nanoparticle pore diameters. The results of the HR-TEM study are found to be in consistency with those of the BET and ESEM analyses. After MG sorption, the pores were filled with MG dyes and the size of the pores was reduced, which supported effective sorption. The development of holes of this size on the AC surface may be the result of carboxylic group treatment followed by wet attrition, which produced the ionized adsorption sites necessary for effective dye adsorption.

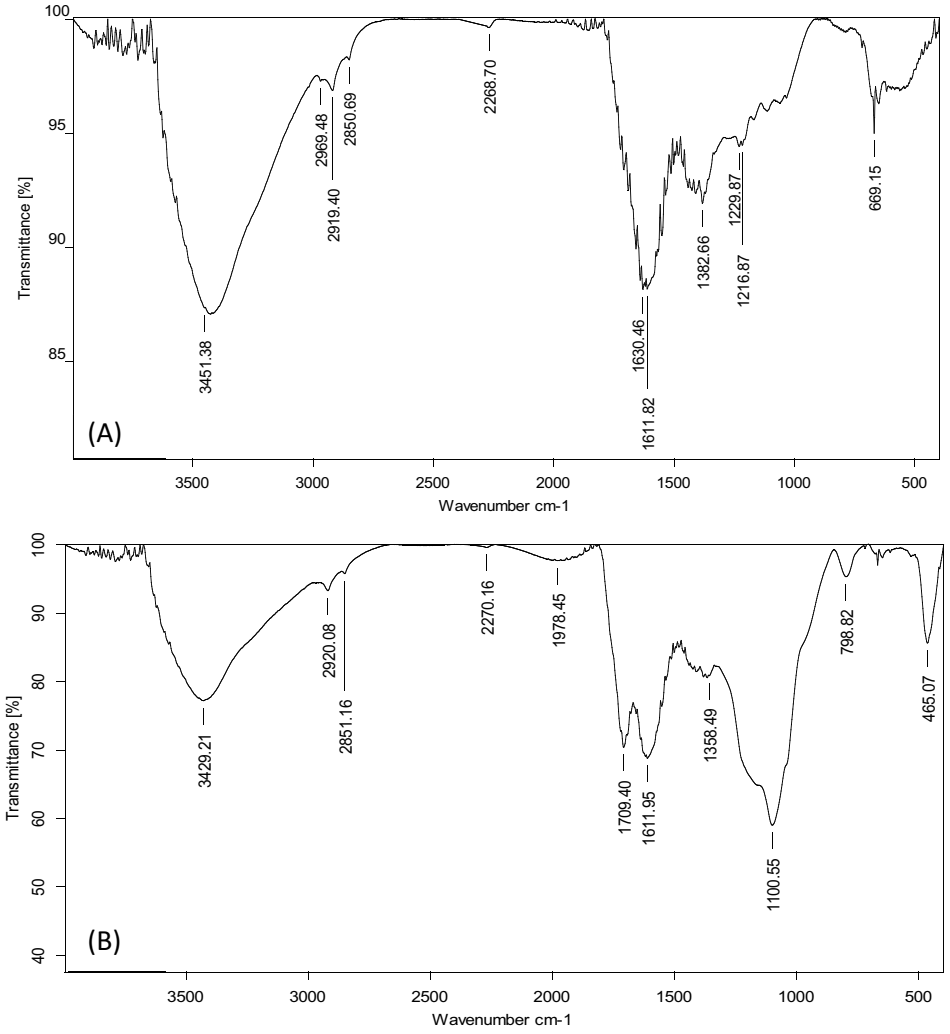

Fig. 2. Fourier-transform infrared spectroscopy routine spectrum for (a) MCGT-AC (b) Malachite green loaded MCGT-AC.

3.2. Mechanism for adsorption

In general, using NaOH to activate carbon surfaces for use as adsorbents is less costly and environmentally dangerous than using other chemicals for the same procedure [31]. During the alkaline activation process, the hydroxide anions interact with the functional groups present on the sorbent carbon surface. According to XEDS analysis, the synthesised chemical is mostly made of carbon (C), oxygen (O), and sodium (Na). This research supports the existence of NaOH infusion in the generated AC. When the surface of the AC is treated with carboxylic groups, carbonate groups develop on the surface, increasing the AC's overall capacity for dye removal. The same is confirmed by HR-TEM study, from which it is obvious that basic group formation on carbon surface have facilitated creation of a significant number of active pores available for adsorption. This can be attributed to oxidation and initiation of redox reaction on the AC surface, which might have caused disunion and detachment of AC surface layers, creating mesoporous surface having large surface area [32]. As a result, the availability of hydroxyl (OH) groups on the surface of the modified AC increased its ability to bind dye molecules by forming hydrogen bonds between the OH groups there and the dye molecules [33]. Additionally, treatment with a carboxylic group will cause the creation of a positive charge ($–COOH^+$) on the sorbent surface as a result of the deposition of an H^+ charge in a solution that is mostly acidic on the surface. This effect causes cationic dye adsorption on a basic surface to increase. However, as the pH of the solution rises, the carboxylic group will exhibit an amphoteric nature (–COOH) and will therefore have an affinity to exchange basic dye molecules with protons. As the pH of the solution rises, the carboxylic group will also become ionised ($–COO^-$), which will eventually encourage the sorption of cationic dye onto AC surfaces (MCGT-AC). Fig. 3 is used to depict the adsorption mechanism. Additionally, it is clear from the comparison of the FTIR spectra of MCGT-AC before and after adsorption (Figs. 2a and b) that the peak for the carboxylic group's frequency changed from 1,630.46 to 1,709.40 cm^{-1}. As a result, the peak's intensity after adsorption was decreased as a result of the deposition of MG molecules on the adsorbent surface. This confirms our assumption, which is validated by characterization investigations, that carboxylic active groups have actively engaged in the sorption system.

3.3. Influence of pH, point of zero charge and zeta potential

Fig. 4 shows how the pH affects the rate of removal and adsorption of MG onto MCGT-AC. Fig. 4a illustrates how the MG adsorption on MCGT-AC benefited from the alkaline condition. Fig. 4b shows the adsorption capacities of MG at pH 7, for which the corresponding adsorption capacity values were found to be 61.63, 161.82, and 198.74 mg/g, respectively, for starting MG concentrations of 25, 50, and 75 mg/L, while for the same dye concentrations, at pH 9.0, MG adsorption values of 62.52, 164.92, and 209.23 mg/g were reported. Observations revealed that, raising the pH value improved both the rate and the capacity of MG adsorption.

The pH of the dye solution regulates ionization for all chemicals and MCGT-AC mass surfaces that are present in the solution mix [34,35]. If the pH of the solution is low, oxygen-containing functional groups on MCGT-AC and carboxylic groups' electronegativity on AC will not be as effective at dissociating hydrogen ions (H^+), and the electrostatic attraction force between the dye cation and MCGT-AC will be weak. In addition, it's possible that free hydrogen ions reduced the pace at which MG was eliminated by competing with the dye cation for adsorption on the AC site. The amount of hydroxide ions in the solution increased as the degree of cationic dye dissociation reduced, and as a result, the rate of cationic dye removal improved as the pH value increased [36]. Additionally, when the pH of the solution increased, the H^+ ion's dissociation on the MCGT-AC surface increased, increasing the adsorbent surface's electronegative character and promoting the electrostatic sorbate–sorbent interaction between the cationic dye and MCGT-AC surface [16]. Moreover, the adsorbent's capacity to bind to molecules in an aqueous medium with a high pH can be improved by the inclusion of a number of active functional agents such carboxyl and hydroxyl groups on the sorbent surface [37]. As a result, MCGT-AC have a high capacity for cationic dye adsorption in an alkaline environment. Similar results have previously been reported [9]. Another result showed that the cationic dye removal adsorption rate increased greatly from pH 2 to 7 and hardly between pH 7 and 9. Another study [38] examined the impact of pH on the cationic dye adsorption by a number of ACs and discovered that when the beginning pH rose, the dye's adsorption capacity increased.

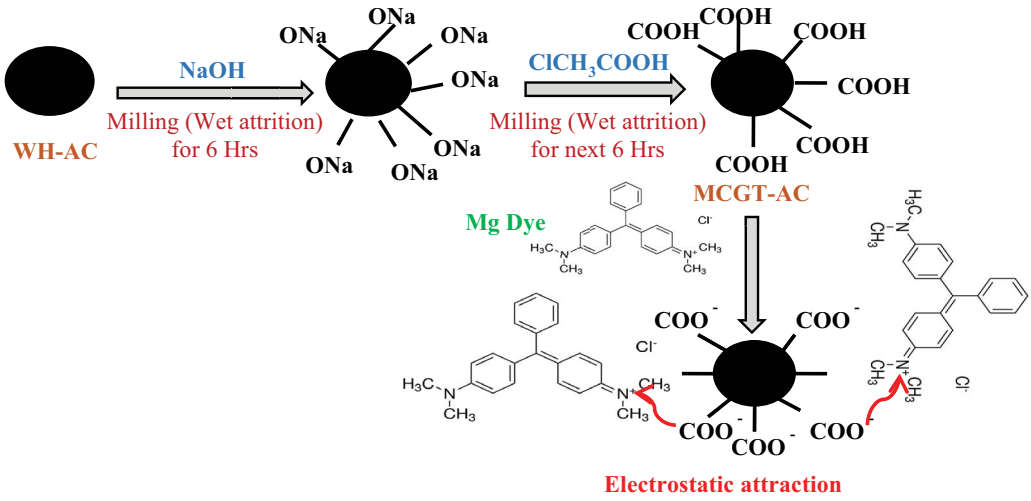

Fig. 3. Adsorption mechanism for Malachite green onto MCGT-AC.

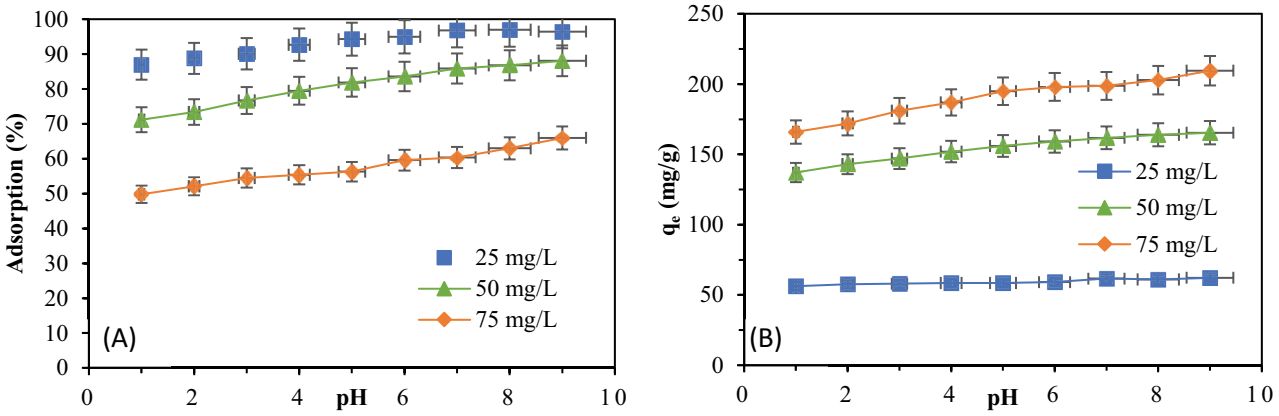

Fig. 4. (a) Sorption rate and (b) sorption capacity for Malachite green onto MCGT-AC at T = 308 K, contact time = 120 min and adsorbent dose = 0.15 g/L.

In section 2.6 of this paper, the zeta potential determination technique is discussed. As per analysis of the zeta potential, the estimated values for MCGT-AC and WH-AC were found to be 4.23 and 5.64, respectively.

A study revealed that WH-AC and MCGT-AC exhibited different surface electronegativities with the later having the higher electronegativity compared to the former one. This was ascribed to the carboxylic group's hydrophobic alkyl end's van der Waals force connection to the activated carbon's nonpolar surface. To lessen the amount of dissociated H^+, carboxylic groups were added to the AC surface along with oxygen-available functional groups including phenolic hydroxyl and carboxyl. Compared to WH-AC, MCGT-AC has a stronger electrostatic affinity and capacity for adsorption towards MG due to its higher electronegativity. Zeta potential study revealed that MG adsorption onto MCGT-AC was stable in a pH range of around 4.2–7.5.

The starting pH was used as a reference point for computing the positive and negative ΔpH ($pH_f - pH_i$) values for the MCGT-AC composite. As per analysis, at an initial pH of 5.5, (pH_{PZC} = 5.5), pH was 0. As a result, when the solution pH is greater than 5.5, as mentioned in section 2.6 of this study, negative charge will predominate on the MCGT-AC surface complex, promoting the adsorption of cationic dye on the adsorbent surface [39,40]. A pH value of 6.5 was taken into consideration for future analysis based on the results of the pH_{PZC} and zeta potential experiments.

3.4. Influence of contact time

Fig. 5 shows the relationship between dye adsorption rate against contact time and dye adsorption capacity against contact time for MG sorption onto MCGT-AC for three initial MG concentrations of 25, 50, and 75 mg/L.

Fig. 4 demonstrates how the removal effectiveness and adsorption capacity of MG onto MCGT-AC increased along with the rise in contact length, finally reaching a maximum value. There were two parts to the operation. Within 30 min of the sorption interaction, the relative adsorption equilibrium state was reached. This performance was caused by the interaction of MG dye molecules with the active basic group sites on the sorbent surface, and the high sorption capacity indicated that most of the functional groups on the MCGT-AC surface had been efficiently and completely occupied by dye molecules. The dye absorption rate was first controlled by the speed at which the dye was transported from the solution to the surface of the adsorbent particles. The second phase was the slow adsorption procedure (for interaction after 30 min). After 30 min of contact time, the relative increase in MG removal extent was negligible, and as time went on, the adsorption rate decreased until it eventually stabilized. The interaction between the MG dye molecules and the adsorption active sites led to the saturation of the functional groups of the MCGT-AC adsorbent. The process of dye particles moving from the MCGT-AC complex's exterior to interior pores controlled the dye adsorption mechanism in the second phase [41]. Additionally, the adsorption equilibrium was achieved more quickly the lower the starting dye concentration. The results mostly agreed with past studies on dye clearance rates [42]. An interaction period of 120 min was taken into consideration for the experiments to determine the maximal adsorption capacity based on the association between contact duration and MG removal.

3.5. Influence of MCGT-AC dose

The dose of the adsorbent has a significant impact on the adsorption processes. Fig. 6 illustrates the examination of 100 mL volumes for each of the three MG concentrations of 25, 50, and 75 mg/L at a solution pH of 7.0, contact period of 30 min, and temperature of 308 K with various adsorbent dosages (5–100 mg). The results showed that as the MCGT-AC adsorbent dosage was increased, the dye removal percentage rose as well. When the dosage of the adsorbent was increased from 5 to 100 mg, the dye removal efficiency increased from 26.2% to 87.5% at a dye concentration of 50 mg/L. This is because the larger dosage's greater surface area provides more MG molecules with active sites to adsorb [43,44].

As the mass of adsorbents increased, more pores and adsorption sites were created, which led to an increase in

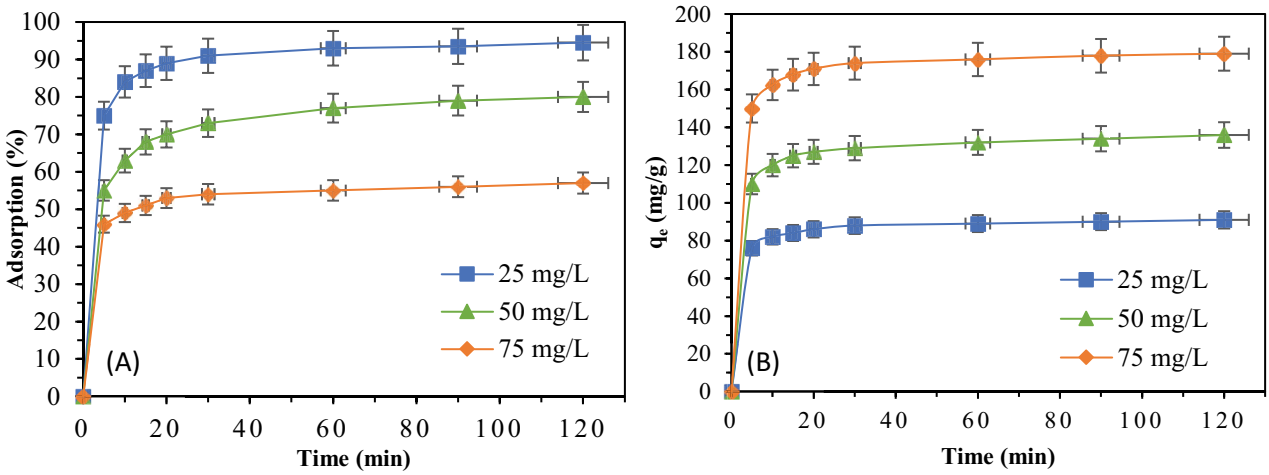

Fig. 5. Influence of contact time for Malachite green adsorption onto MCGT-AC (a) sorption rate and (b) sorption capacity, with MCGT-AC dose = 0.15 g/L and pH = 6.5.

the removal rate of MG. When the adsorbent dosage was increased to a specific level, the adsorption rate would tend to approach equilibrium. With regard to dye removal percentages of 83.6%, 87.5%, and 93.4%, which correspond to initial MG concentrations of 25, 50, and 75 mg/L, the MG removal rate began to approach saturation at adsorbent masses of 35, 55, and 85 mg. The quantity of dye concentration in the solution stays the same for any given dye concentration value even though we keep upping the adsorbent dosage. Because not enough dye molecules were present in the solution to occupy all of the potential active adsorptive sites at higher adsorbent dosages, saturation of adsorption occurred. In other words, equilibrium adsorption rate was reached, which suggests that as sorbent dose increased, adsorption capacity gradually decreased before the adsorption process stabilised.

3.6. Influence of initial MG concentration

The impact of different beginning dye concentrations (25, 50, 75, and 100 mg/L) on the removal of MG dye was examined using the same quantity of MCGT-AC (5–100 g) and adjusting the dye solution pH at 7. Adsorbent samples of 15 mg were added to a 100 mL dye solution and heated to 308 K for 120 min to complete the process. The test results are displayed in Table 3.

According to the results shown in Table 3, as the starting dye concentration was increased from 25 to 100 mg/L, the sorption rate (percent) of MG by 15 mg of MCGT-AC adsorbent decreased from 96.7% to 53.2%, but at the same time, the equilibrium sorption capacity (q_e) increased from 63.9 to 171.3 mg/g for the same increase in dye dose. In fact, if we pay close attention, the highest adsorption capacity value of 169.8 mg/g was attained at an adsorbent dose of 75 mg/L. When we increased the MG dose further at 100 mg/L, total adsorbed dye molecule quantity may have been higher, but the rate of adsorption decreased to 167.3 mg/L. This suggests that dosage of 75 mg/L was optimal for adsorption of dye, which is proven by highest adsorption capacity.

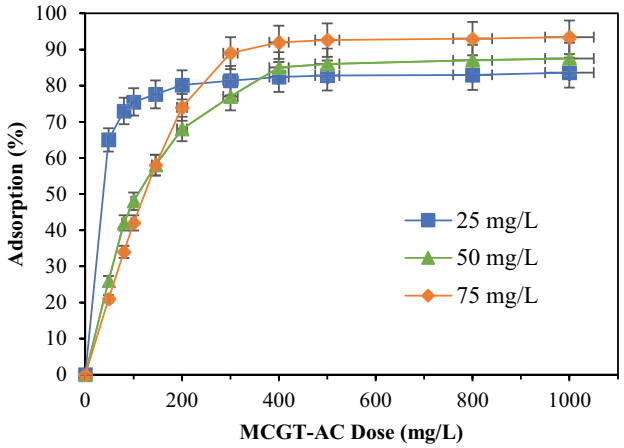

Fig. 6. Influence of sorbent dose on dye removal (temp = 308 K, pH = 7.0 and time = 30 min).

The degree of dye removal decreased as the initial MG concentration increased due to a lack of accessible active sites under high concentration conditions of MG [45]. However, as the original MG concentration rose, so did the MG's ability to adsorb onto MCGT-AC. Carboxylic modified functional groups provided favourable ion exchange sites for the adsorption of MG ions. Activated carbon treated with NaOH and chloroacetic acid followed by attrition exhibits more positively charged adsorption sites and a sizable capacity to remove cationic dyes when compared to untreated AC [24].

3.7. Adsorption kinetics

For every sorbate–sorbent interaction, kinetic research is concerned with the reaction rate and reaction limiting phases. For the current dye adsorbent interaction system, kinetics was examined using five distinct models (viz. pseudo-first-order, pseudo-second-order, Elovich, modified Freundlich and intraparticle diffusion model) in order to investigate the closeness. The coefficient correlation (R^2) value was used to evaluate the fit between actual data from experiments and computed data from different models. The better a model fits the real experimental data, the closer its R^2 values are to unity.

According to the pseudo-first-order kinetic model, adsorption is regulated by diffusion processes, and the rate of reaction is proportional to the number of ions still present in the solution [33]. It is believed that the adsorption rate is connected to the discrepancy between the saturation concentration and the quantity of MCGT-AC that has been absorbed throughout time. The following equation displays the integral Eq. (3).

$$\ln\left(q_e - q_t\right) = \ln q_e - k_1 t \tag{3}$$

where q_e is the equilibrium dye adsorption quantity (mg/g), q_t is the dye adsorption capacity at time intervals t (in mg/g),

Table 3
Dye concentration vs. percentage removal

Dye concentration (mg/L)	MCGT-AC		WH-AC	
	Adsorption percentage (%)	Adsorption capacity (mg/g)	Adsorption percentage (%)	Adsorption capacity (mg/g)
25	94.6	61.7	79.5	50.3
50	88.3	116.4	68.4	92.8
75	85.7	169.8	63.7	127.6
100	51.4	167.3	47.1	126.9

and k_1 is the adsorption rate constant (min^{-1}). The rate constant in this model was determined using the slope of the $\ln(q_e - q_t)$ plot over time (t). The calculated R^2 values were between 0.845 and 0.969 (Table 4). Further evidence that the pseudo-first-order model failed to adequately explain the adsorption process came from the stark differences between the $q_{e,exp}$ and $q_{e,cal}$ values.

The rate of reaction for the sorbate–sorbent interaction is equivalent to the concentration of the reactants under consideration, assuming that chemical adsorption is the dominating force, according to the kinetic model for pseudo-second-order rate of reaction indicated in Eq. (4).

$$\frac{t}{q_t} = \frac{1}{K_2 q_e^2} + \frac{1}{q_e} t \tag{4}$$

where K_2, which may be computed for different concentrations using curves of t/q_t vs. t, is the constant for reaction rate corresponding to second-order kinetic given as g/mg·min (Fig. 7a). All of the temperature studies that showed excellent match for the experimental data had estimated correlation coefficients (R^2) in the range of 0.998 to 0.999. The experimental q_e that differ from the calculated ones are listed in Table 4. Based on the results obtained using the pseudo-second-order kinetic model, it is obvious that the theoretical $q_{e,cal}$ and the experimental $q_{e,exp}$ were in good agreement, indicating the applicability of the model.

For any system, intraparticle diffusion proceeds inro two phases, in the first step, dye molecules shift from solution mix to the adsorbent surface, in the second phase, dye molecules diffuse into the internal pores [43]. To analyse influence of intraparticle diffusion, Weber–Morris model is used which may be expressed as in Eq. (5).

$$Q_t = K_{ip} t^{1/2} + C_i \tag{5}$$

where K_{ip} is the rate constant for intraparticle diffusion expressed as (mg/g·$min^{1/2}$) and C_i is the constants for layer of boundary thickness with unit as mg/g, which may be determined from the plot of Q_t vs. $t^{1/2}$. C_i values can be obtained from the intercepts of the linear lines with the Y-axis, obtained for the plot. The constant C_i (80.9, 100.09, 114.02) was observed to grow as the MG dye concentration increased, possibly due to a thickening of the boundary layer (Table 4). Greater intercept values of C_i suggested that at the early phases of the intraparticle diffusion, exterior diffusion of the MG particles was controlling the adsorption. The early diffusion pattern also showed that the data fitting the model do not pass through the origin, hinting that intraparticle diffusion wasn't the sole mechanism involved in the sorption process and other sorption rates are also participated in the sorption mechanism. However, the closeness of R^2 values with unity indicates that the intraparticle model is having a role in the sorption process.

Eq. (6), which represents adsorption in a non-ideal condition, was used to express the Elovich model for the process. As per the model, adsorption process is split into two categories: quick adsorption and slow adsorption.

$$Q_t = \frac{1}{\beta}\ln(\alpha\beta) + \frac{1}{\beta}\ln(t) \tag{6}$$

Table 4
Kinetic parameters for different models

Model constants	Concentration (mg/L)		
	25	50	75
	$q_{e,exp}$ (mg/g)		
	182.9	216.4	251.6
Pseudo-first-order			
$q_{e,cal}$ (mg/g)	91.4	108.2	143.1
K_F (min^{-1})	0.0085	0.0149	0.0069
R^2 (linear)	0.856	0.889	0.953
Pseudo-second-order			
$q_{e,cal}$ (mg/g)	182.1	212.6	245.5
h (mg/g·min)	1.431	1.245	1.754
K_s (min^{-1})	0.582	0.541	0.483
R^2 (linear)	0.999	0.998	0.998
Elovich model			
β (g/mg)	7.562	6.224	6.864
α (mg/g·min)	8.23×10^5	0.476	2.97×10^8
t_0	1.009×10^{-5}	1.097	2.991×10^{-8}
R^2 (linear)	0.852	0.981	0.985
Modified Freundlich			
m	0.437	0.361	0.253
k (dm^3/g·min)	0.476	0.167	0.384
R^2 (linear)	0.957	0.880	0.899
Intraparticle diffusion			
K_{ip}	3.78	4.56	4.89
C_i	80.9	100.09	114.02
R^2	0.917	0.946	0.936

where β is the desorption coefficient (mg/g) and α is the initial adsorption rate (mg/g·min). Q_t vs. ln$t$ is represented with a line with intercept value of 1/β ln(αβ) and slope value of 1/β. At MG concentrations of 25, 50, and 75 mg/L, the correlation coefficient (R^2) was found to be 0.852, 0.981, and 0.985, respectively (Fig. 7c). For MG concentration of 25 mg/L, actual data from experimentations do not fit well with the calculated data from the models.

However, the fact that the experimental data were effectively compared by the Elovich model at starting MG concentrations greater than 25 mg/L revealed that the intraparticle diffusion mechanism was the rate-limiting phase, but not the only one [46,47].

Kuo–Lotse were the first to establish the modified Freundlich equation (1973). It is written as follows:

$$q_t = kC_0 t^{1/m} \tag{7}$$

where q_t represents the adsorbed dye quantity in mg/g for any given time t, k represents the constant for rate of reaction for the sorption system in mg/g, C_0 represents the dye concentration at the starting stage in mg/L, m represents

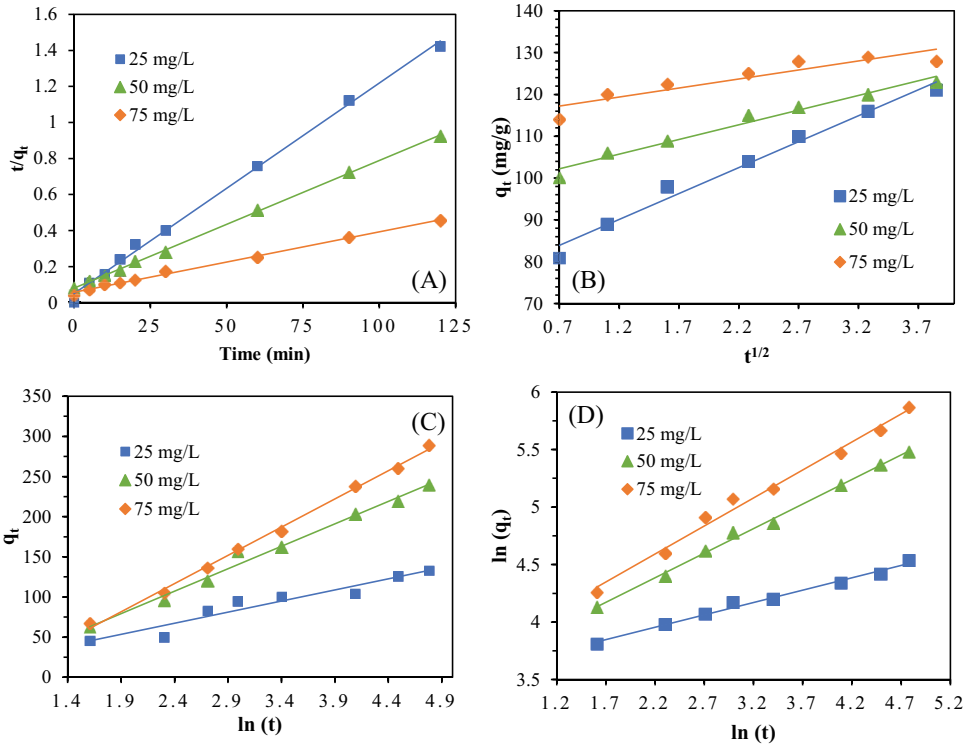

Fig. 7. Kinetic plots for (a) pseudo-second-order, (b) intraparticle diffusion, (c) Elovich kinetic model and (d) modified Freundlich rate kinetic.

the constant by Kuo–Lotse model. The modified Freundlich equation is written in linear form as:

$$\ln q_t = \ln\left(kC_0\right) + \frac{1}{m}\ln t \tag{8}$$

Fig. 7d shows the constants determined for modified Freundlich model from the graph of $\ln q_t$ vs $\ln t$. Along with other kinetic constants, all the modified Freundlich model constants are presented using Table 4. Results suggest that experimental data do not fit this model well.

Kinetic analysis reveal that pseudo-second-order model fitted best with actual experimentation data and therefore sorption system was regulated by chemical adsorption phenomenon. In addition to intraparticle diffusion and micropore internal diffusion, adsorption mechanism was also supported by chemical sorption, where, electron interaction happened among the dye sorbate and MCGT-AC sorbent and subsequent exchange, release and acceptance of electrons occurred among them [48].

3.8. Isotherm analysis

To understand the sorbate–sorbent interaction nature of any adsorption system, fitting the experimental data with various models defining the equilibrium adsorption stage is of primary importance. To know, how the system reaches to its equilibrium capacity is of utmost importance to understand the underlying sorption mechanism of that particular system. Several such models are used in this study to understand the equilibrium data of the sorption process. The experimental equilibrium adsorption data for MG adsorption onto MCGT-AC was assessed using the Langmuir, Toth, Freundlich, Dubinin–Radushkevich, Temkin, Radke–Prausnitz and Redlich–Peterson isotherm models. Representative equations for the models are presented [49,50]:

$$\text{Freundlich, } q_e = K_F C_e^{1/n} \text{ or } \ln q_e = \ln K_F + \left(\frac{1}{n}\right)\ln C_e \tag{9}$$

$$\text{Langmuir, } q_e = \frac{q_m b C_e}{1 + bC_e} \text{ or } \frac{C_e}{q_e} = \left(\frac{1}{q_m b}\right) + \frac{C_e}{q_m} \tag{10}$$

$$\text{Temkin, } q_e = B_T \ln K_T + B_T \ln C_e \tag{11}$$

$$\text{Redlich-Peterson, } q_e = \frac{K_R C_e}{1 + a_R C_e^{\beta}} \text{ or } \ln\left(K_R \frac{C_e}{q_e} - 1\right) = \ln a_R + \beta \ln C_e \tag{12}$$

$$\text{Toth, } q_e = \frac{q_{\text{Th}} C_e}{\left(1/K_{\text{Th}} + C_e^{\text{Th}}\right)^{1/\text{Th}}} \text{ or } \left(\frac{C_e}{q_e}\right)^{\text{Th}} = \frac{1}{\left(q_{\text{Th}}\right)^{\text{Th}} K_{\text{Th}}} + \frac{\left(C_e\right)^{\text{Th}}}{\left(q^{\text{Th}}\right)^{\text{Th}}} \tag{13}$$

$$\text{Redke-Prausnitz, } q_e = \frac{K_{\text{RP}} K_{\text{RP}} C_e}{1 + K_{\text{RP}} C_e^{P}} \text{ or } \frac{C_e}{q_e} = \frac{1}{K_{\text{RP}} k_{\text{rp}}} + \frac{C_e^{P}}{k_{\text{rp}}} \tag{14}$$

$$\text{Dubinin-Radushkevich}\left(D-R\right), \ln q_e = \ln q_m - K\varepsilon^2 \quad (15)$$

$$\varepsilon = RT \times \ln\left[1+\left(\frac{1}{C_e}\right)\right] \quad (16)$$

$$E_m = \frac{1}{\sqrt{2K}} \quad (17)$$

For surface of adsorbents with heterogeneity and irregular heat of adsorption distribution throughout the surface, the Freundlich isotherm holds true. The Langmuir isotherm, on the other hand, posits that sorption occurs at homogenous locations and formation of monolayer on the adsorbent surface. The isotherms of Redlich–Peterson, Toth, and Radke–Prausnitz, on the other hand, may be used in both homogeneous as well as heterogeneous systems, whereas Dubinin–Radushkevich isotherm gives a fair idea about physical and/or chemical adsorption nature of the process.

Table 5 shows the various parameter values for the isotherms studied for MG dye adsorption onto MCGT-AC.

Table 5
Isotherm constants for Malachite green sorption onto MCGT-AC

Isotherm model	Constants	Temperature, K		
		298 K	308 K	318 K
Langmuir	q_m (mg/g)	187.8	221.5	251.6
	b (L/mg)	4.245	6.915	7.412
	R_L	0.324	0.416	0.421
	R^2	0.998	0.999	0.999
Freundlich	K_F (mg/g)	10.56	12.96	14.87
	n	5.34	6.78	7.13
	$1/n$	0.213	0.209	0.204
	R^2	0.976	0.979	0.978
Temkin	B_T	0.292	0.324	0.379
	K_T (L/mg)	54.678	57.141	75.221
	R^2	0.974	0.973	0.973
Redlich–Peterson	a_R (L/mg)	1	1	1
	K_R (L/mg)	3.827	3.215	3.977
	β	0.971	1.003	1.002
	R^2	0.978	0.979	0.979
Toth	Th	0.958	0.968	0.965
	q_{einf} (mg/g)	2.686	2.474	2.518
	K_{Th} (mg/L)Th	2.599	2.212	2.458
	R^2	0.963	0.956	0.957
Radke–Prausnitz	P	0.932	0.942	0.923
	K_{RP} (L/g)	9.250	4.262	4.462
	K_{rp} (mg/g)/(mg/L)$^{1/P}$	1.531	1.690	1.774
	R^2	0.947	0.947	0.948
Dubinin–Radushkevich	q_m	174.2	184.6	194.7
	E_m (kJ/mol)	33.41	46.42	50.18
	K (mol^2/J^2) × 10^3	4.67	5.12	7.98
	R^2	0.984	0.985	0.987

Nonlinear regression analysis was used with Excel 2007's solver-add-in tool to evaluate various parameters by using the experimental data into respective model equations.

In the Langmuir model, C_e is dye conc. in solution at equilibrium in mg/L, q_e is adsorption capacity at equilibrium in mg/g, Langmuir constant is represented using q_m in mg/g, b in L/mg signifies the rate of adsorption for Langmuir isotherm. The R^2 value derived from the plot of C_e/q_e vs. C_e was in the range of 0.998–0.999 (Table 5), demonstrating that the adsorption process is well described using the Langmuir isotherm model (Fig. 8a). R_L describes the feasibility of adsorption process, which can be expressed using Eq. (18) as [51]:

$$R_L = \frac{1}{1+bC_0} \quad (18)$$

where the starting dye concentration in the solution is represented using C_0 (mg/L). The isotherm feasibility is determined from the value of R_L, if condition is $0 < R_L < 1$, sorption is favourable, $R_L = 0$ means irreversible process, not feasible if $R_L > 1$ and linear when $R_L = 1$. For the present analysis, the R_L value of MG adsorption was in the range of 0.324–0.421. It is indicative that the adsorption procedure was favourable (water paper). As per Langmuir modelling, maximum theoretical capacity of adsorption for MG onto MCGT-AC was evaluated to be 251.6 mg/g, whereas the same corresponding value for MG onto WH-AC was found to be 143.6 mg/g.

For Freundlich model, $1/n$ and K_F values symbolizes sorption potential values. Greater the magnitude of $1/n$, greater is the attraction and heterogeneity between the among adsorbent and adsorbate. Table 5 shows that K_F values rise as temperature rises, suggesting increased dye absorption by MCGT-AC at elevated temperatures, at the same time suggesting that system adsorbed heat from the system supporting endothermic adsorption. The $1/n$ numbers represent the comparative energy site distribution and are dependent on the adsorption process's kind and strength. Since $1/n < 1$, MG dye is preferentially absorbed by MCGT-AC at all temperatures. The heat of dye adsorption onto MCGT-AC is linked to the Temkin constant (B_T). In all circumstances, B_T increases as the temperature rises. The sorbate sorbent interaction is accounted by the Temkin constant, K_T. On the other hand, homogeneity and heterogeneity of the sorption system is analysed using the three parameters of the Redlich–Peterson model. Except at 298 K, for MG sorption, β = 1 suggests favourable adsorption at higher temperatures. The system's heterogeneity is also represented by the Toth isotherm exponent (Th), which is generally lower than unity. As constant Th diverge away from unity, the adsorbent's heterogenic nature rises, and as Th reaches unity, Toth model converges with the concept of Langmuir isotherms. Similarly, for Radke–Prausnitz model, as P-value approaches to unity, the same converges with the concept of Langmuir model. E_m (mean free energy) gives a fair idea about the sorption nature of the system, if E_m value is within 8 kJ/mol, process will follow physical adsorption. If the same value is determined to be in the range of 8 to 16 kJ/mol, the system is assumed to be being controlled by ion-exchange process and if the

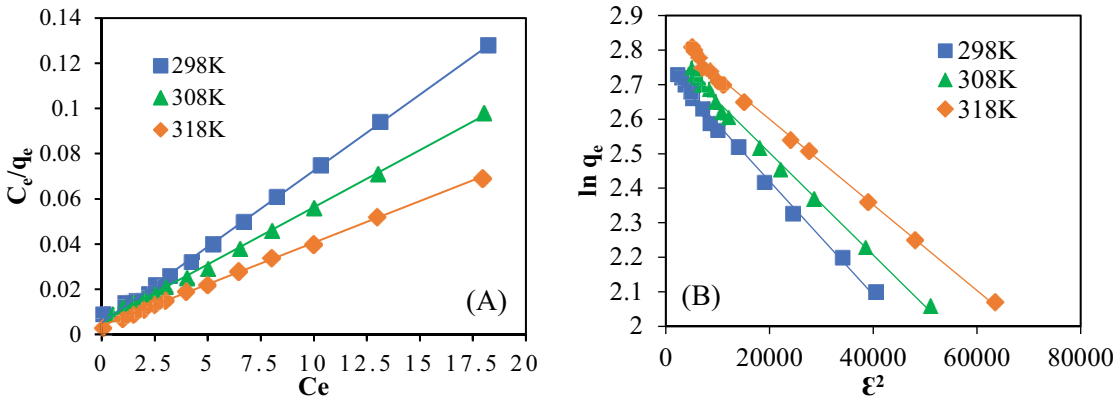

Fig. 8. Isotherm plots for (a). Langmuir model and (b) Dubinin–Radushkevich model (MCGT-AC dose = 0.15 g/L, pH = 6.5, and C_0 = 25–75 mg/L).

E_m value evaluated, comes out in the range of 16 to 400 kJ/mol, the system will follow chemical adsorption. E_m values in the current system were 33.41, 46.42 and 50.18 kJ/mol at 298, 308, and 318 K, indicating chemical adsorption.

The Langmuir, Dubinin–Radushkevich and Redlich–Peterson models in order of their mention, all demonstrated their suitability for the experimental equilibrium data, with Langmuir equation showing closest proximity. Study of isotherms suggested that adsorbate–adsorbent interaction was a monolayer affair. On the other hand, proximity of second fitted Dubinin–Radushkevich model supported the feasibility of chemical adsorption. Carboxylic treatment followed by mechanical attrition on the MCGT-AC surface resulted in a homogenous pore distribution over the AC surface, resulting in homogeneous adsorption sites. From the results of the kinetic and isotherm investigations, inference can be drawn that adsorption mechanism of cationic dye onto MCGT-AC followed chemical monolayer adsorption.

3.9. Analysis of error function

A vast amount of data from the investigation of dye adsorption by MCGT-AC was evaluated on multiple linearized models in order to find the best fit model. But due to the linearization inherent bias resulted and sets of different isotherm parameters were established using non-linear regression equations. Using the original form of the isotherm equation, this gives a mathematical approach for calculating the isotherm parameters. So, the optimization approach requires an error function to match the isotherm data to the experimental equilibrium data. Because the error function chosen has an impact on the parameters of the derived-error function, which is mostly based on absolute deviation bias, the data fits into a zone of high concentration. This weighting is increased even more when extreme errors are penalized by the square of the deviation. The bias can be counterbalanced by dividing the deviation with the help of a computed value to demonstrate the relevance of fractional deviation. Isotherm parameters were identified through the analysis of error function isotherms by minimizing the corresponding error functions over the concentration range using the Solver add-in for Microsoft Excel. This program's initialization is based on a clever guess parameter. In Microsoft Excel, an iterative procedure was started using the numbers obtained from the linearized version of the model. The following sections detail the various error functions. Error analysis data is presented using Table 6.

3.9.1. Sum of the absolute errors

The sum of the absolute error's method can be given by the equation:

$$\mathrm{SAE} = \sum_{i=1}^{n} \left| q_{e,\exp} - q_{e,\mathrm{cal}} \right|_i \tag{19}$$

where $q_{e,\exp}$ is the adsorbate concentration that was adsorbed during the experiment, which was calculated from the concentration of equilibrium sorbate liquid phase, C_e was achieved experimentally, and $q_{e,\mathrm{cal}}$ is the concentration of theoretical solid phase of sorbate that was adsorbed onto the sorbent, which was calculated using one of the isotherm equations. The data of the error function is raised by biassing the fit towards the zone of high concentration, which is done by using error functions to determine isotherm parameters.

3.9.2. Sum of squared errors

The sum of squared errors (SSE) method can be written as follows:

$$\mathrm{SSE} = \sum_{i=1}^{n} \left(q_{e,\mathrm{cal}} - q_{e,\exp} \right)_i^2 \tag{20}$$

As the square of the amount of error grows, the isotherm parameters computed using this error function give a better fit, resulting in a biassing of fit towards data gathered at the upper end of the concentration range. Despite being the most often used error function, the error function has a number of drawbacks.

3.9.3. Hybrid fractional error function

The sum of the square of the error is divided by the measured value to best suit the sum of the square of the

Table 6
Error functions for Malachite green sorption onto MCGT-AC

Isotherm	Error functions	Temperature		
		293	303	313
Langmuir	SAE	0.293	0.252	0.241
	SSE	0.018	0.015	0.013
	HYBRID	1.381	0.891	0.887
	MPSD	3.424	3.746	3.587
	ARE	3.642	2.879	2.471
	χ^2	0.005	0.006	0.006
Freundlich	SAE	0.248	0.347	0.378
	SSE	0.054	0.035	0.047
	HYBRID	1.675	0.008	–0.024
	MPSD	4.781	6.645	6.742
	ARE	2.997	3.745	4.014
	χ^2	0.017	0.024	0.075
Temkin	SAE	0.247	0.279	0.279
	SSE	0.017	0.026	0.028
	HYBRID	–0.245	–0.324	–0.279
	MPSD	4.371	5.472	5.875
	ARE	2.745	2.579	3.478
	χ^2	0.008	0.014	0.017
Redlich–Peterson	SAE	0.245	0.257	0.278
	SSE	0.012	0.014	0.013
	HYBRID	–0.214	–0.113	–0.152
	MPSD	3.984	4.254	3.124
	ARE	2.278	2.314	2.007
	χ^2	0.008	0.009	0.009
Toth	SAE	0.234	0.245	0.241
	SSE	0.013	0.014	0.012
	HYBRID	–0.124	–0.134	–0.213
	MPSD	4.523	4.278	3.124
	ARE	2.642	2.548	2.354
	χ^2	0.009	0.009	0.014
Radke–Prausnitz	SAE	0.254	0.423	0.246
	SSE	0.014	0.086	0.024
	HYBRID	–3.245	–3.423	–0.247
	MPSD	4.785	6.245	5.247
	ARE	3.124	5.247	2.578
	χ^2	0.014	0.024	0.013
Dubinin–Radushkevich	SAE	0.124	0.243	0.238
	SSE	0.011	0.013	0.012
	HYBRID	–0.217	–0.115	0.175
	MPSD	4.017	4.245	3.241
	ARE	2.195	2.297	2.010
	χ^2	0.008	0.008	0.009

error at a very low concentration. Porter et al. created an error function to achieve this better match. In the isotherm equation, it also employs the number of data points minus the number of parameters (n–p) and the number of degrees of freedom of the system as a divisor. It is written as follows:

$$\text{HYBRID} = \frac{100}{n-p}\sum_{i=1}^{n}\left[\frac{q_{e,\text{exp}} - q_{e,\text{cal}}}{q_{e,\text{exp}}}\right]_i \tag{21}$$

3.9.4. Marquardt's percent standard deviation

It is represented as:

$$\text{MPSD} = 100\sqrt{\frac{1}{n-p}\left\{\sum_{i=1}^{n}\left(\frac{q_{e,\text{exp}} - q_{e,\text{cal}}}{q_{e,\text{exp}}}\right)_i^2\right\}} \tag{22}$$

This error function has already been used by a lot of scholars in this field. It is similar to the geometric mean error distribution, which improves as the number of degrees of freedom of the system increases.

3.9.5. Average relative error

The average relative error (ARE) function is calculated as follows:

$$\text{ARE} = \frac{100}{n}\sum_{i=1}^{n}\left[\frac{q_{e,\text{exp}} - q_{e,\text{cal}}}{q_{e,\text{exp}}}\right]_i \tag{23}$$

Throughout the concentration range, this error function strives to maintain the fractional error distribution as minimal as feasible.

3.9.6. Chi-square (χ^2) test

$$\chi^2 = \frac{\left(q_{e,\text{exp}} - q_{e,\text{cal}}\right)^2}{q_{e,cal}} \tag{24}$$

For each squared difference, Chi-square is the sum of the squares of the differences between experimental data and data created from models, divided by the comparable data produced from models. When comparing the fitness of isotherms, the lowest values of χ^2 are used in error analysis and the greatest values of R^2 are used when evaluating the fitness of isotherms. Table 6 demonstrates that the hybrid fractional error values are the lowest when compared to other error functions. The applicability of isotherms for the current investigation, based on the inference of values for error functions (Table 6) and correlation coefficients values for isotherms (Table 5) is determined in the following order: Langmuir > Dubinin–Radushkevich > Redlich–Peterson > Freundlich > Radke–Prausnitz > Toth > Temkin.

As per the fitness, three of the best-fit isotherms (Langmuir and Dubinin–Radushkevich) are shown using Fig. 8a and b, respectively. For Langmuir model, the curve is plotted between C_e/q_e and C_e, for Dubinin–Radushkevich model, plot was drawn between $\ln q_e$ and ε^2.

3.10. Influence of temperature and thermodynamics parameters

Three distinct MG dye concentrations (25, 50, and 75 mg/L) were tested at different temperatures (298, 308,

and 318 K), and the results revealed that MG adsorption onto MCGT-AC increased with increasing temperature suggesting endothermic nature of the adsorption process. The ability to dissolve in solution, thermal movement and chemical reactivity of dye molecules increased as temperature rose [52]. Furthermore, it was shown that structure of pores of AC is closely associated with temperature. As the temperature rose, the size of the pore and quantity of active adsorptive sites of AC expanded due to aided thermal movement. As a result of these factors, sorbate–sorbent interaction increased and consequent enhanced removal of dye onto modified adsorbent with rise in temperature.

In thermodynamics study, effect of temperature and mechanism influencing the sorption process were also discussed. The thermodynamics of MCGT-AC adsorption were explored from an energy viewpoint. The adsorption thermodynamics technique was utilized to study the adsorption driving force and determine if the adsorption process was spontaneous or not. The thermodynamic formulas described in Eqs. (25)–(28) are used to calculate change in entropy (ΔS), change in enthalpy (ΔH) and change in free energy (ΔG) [53]:

$$\Delta G = -RT \ln K_C \tag{25}$$

$$K_C = \frac{q_e}{C_e} \tag{26}$$

$$\ln K_C = \frac{\Delta S}{R} - \frac{\Delta H}{RT} \tag{27}$$

$$\Delta G = \Delta H - T\Delta S \tag{28}$$

where temperature in K is presented using T, R stands for universal gas constant (8.314 J/mol·K), and K_C is for thermodynamic constant. ΔS, ΔH and ΔG stand for change in entropy in kJ/mol·K, change in enthalpy in kJ/mol and change in Gibbs free energy in kJ/mol, respectively. Van't Hoff's plot ($\ln K_C$ vs. $1/T$) was used to calculate ΔH and ΔS values, which are presented using Table 7.

Table 7
Thermodynamic parameters for Malachite green removal onto MCGT-AC

Thermodynamic parameters				
Dye conc. (mg/L)	Temperature (K)	ΔG (kJ/mol)	ΔS (kJ/mol·K)	ΔH (kJ/mol)
25	298	–9.24	0.087	6.59
	308	–11.67		
	318	–12.68		
50	298	–8.43	0.095	10.57
	308	–9.36		
	318	–10.12		
75	298	–5.72	0.098	13.45
	308	–6.34		
	318	–6.92		

The negative ΔG values, as shown in Table 7, proved the spontaneous and feasible nature of MG sorption onto MCGT-AC [54]. The drop in ΔG values as temperature rose suggested adsorption was favourable at elevated temperature [55,56]. At three starting dye concentrations (Table 7), evaluated positive ΔH values of 6.59, 10.57, and 13.45 kJ/mol for corresponding temperatures of 298, 308 and 318 K supported the hypothesis of endothermic nature of the system [57]. For the discussed dye concentrations, positive ΔS values of 0.087, 0.095, and 0.098 kJ/mol·K at 25, 50 and 75 mg/L, were observed suggesting the system was more disordered at equilibrium after adsorption compared to initial stage supporting high adsorption of dye. Positive values of ΔS suggested that higher disorder ness of the adsorption system at higher temperature indicating higher sorbent–sorbate interaction which suggests successful and effective sorption of dye onto modified adsorbent [7].

3.11. Determination of activation energy

Adsorption is possible in a adsorbate–adsorbent interaction if adsorbate particles meet on the surface of the adsorbent with a minimum energy in a specific direction. The adsorbate particle must pass the energy wall present on the adsorbent's surface in order for adsorption to occur. That minimum energy which is required to overcome all the interventions for successful adsorption can be defined as activation energy (E_a). For any sorption system, if the energy of activation comes out to be within 40 kJ/mol, the system will be controlled by physical adsorption, and if E_a value evaluated is >40 kJ/mol, the process will be under the control of chemical adsorption [17]. An empirical relation is given by Arrhenius for this energy:

$$K_{p2} = Ae^{-E_a/RT} \tag{29}$$

where K_{p2} is the constant for rate of adsorption, ideal gas constant is presented using R, constant of proportionality is presented with A that changes according to process, energy for activation is given using E_a, and temperature in K is represented using T.

Applying operation of natural log (at the base e) both the side of Eq. (29) gives the linearized form of the Arrhenius relation as:

$$\ln K_{p2} = \ln A - \frac{E_a}{RT} \tag{30}$$

By plotting the curve of $\ln K_{p2}$ vs. $1/T$, E_a of the system is found out. In relation to Eq. (30), ($-E_a/R$) value is determined using the linear plot derived from the linearized form of the Arrhenius equation. The maximum E_a value evaluated for the system is 51.36 kJ/mol, indicating that the process for the present analysis favours chemical adsorption.

3.12. Isosteric heat of adsorption

For a uniform rate of surface coverage of adsorbent with the adsorbate particles, a heat is generated during adsorbate–adsorbent interaction which may be expressed as isosteric hear for the adsorption process. Clausius–Clapeyron equation can be used to compute the same as:

$$\ln C_e = \left(-\frac{\Delta H_x}{R}\right)\frac{1}{T} + \text{constant} \quad (31)$$

where concentration of the adsorbate at equilibrium is presented using C_e in mg/L, ΔH_x denotes for isosteric heat of adsorption (kJ/mol), ideal gas constant value (8.314 J/mol·K) given by R, and T is the absolute temperature in K. Eq. (31) yields the adsorption isostere in the form of a straight line, and the value of $(-\Delta H_x/R)$ is derived from the plot of $\ln C_e$ and $1/T$. At constant surface loading (SL), the best fitted isotherm model gives the value of C_e. For SL of constant rate, C_e values were obtained from the best fitted isotherm model as per section 3.9 and 3.10 of this article. Accordingly, C_e values were calculated from the Langmuir isotherm for the process and were considered for isosteric heat analysis. Study was conducted for four different surface loadings viz. 10, 12, 14 and 16 mg/g at 298, 308 and 318 K. Result for the same is shown using Fig. 9.

The temperature and the SL are the main factors on which ΔH_x depends. The system behaviour is assumed to be endothermic if isosteric heat for the system rises with rise in temperature. Similarly, if ΔH_x reduces with declination in temperature system behaviour is predominantly exothermic. If adsorbent surface is homogeneous then ΔH_x is independent of the surface loading and will be constant. But if ΔH_x changes with SL, then the sorbent surface is energetically non homogenous which favours adsorption suggesting high lateral affinity among adsorbate molecules. Low magnitude of ΔH_x is result of predominance of adsorbate–adsorbate interaction whereas higher ΔH_x value is due to predominance of adsorbent–adsorbate interaction. A comparison of isosteric heat vs temperature showed increase in isosteric heat against increased temperature supporting endothermic characteristic of the system which is in synchronization with the thermodynamic studies done for this research.

3.13. Regeneration studies

Eluents such as dilute HCl and dilute NaOH and room temperature were being considered to regenerate the used MCGT-AC. Table 8 shows the desorption results for MCGT-AC regeneration with 1.0 M NaOH and initial dye concentration of 10 mg/L, for which sorption capacity reduced from 95.7% to 48.6% at 6th regeneration cycle. Table 9 illustrates the similar results for varied HCl and NaOH concentrations (ranging from 0.2 to 1.0 M). Observations revealed that NaOH with 1.0 M concentration reflected highest regeneration ability, any high concentration value of NaOH was showing detrimental regeneration effect possibly due to residual OH^- on the MCGT-AC or adsorbent structure degradation. As a result, a solution with 1.0 M NaOH concentration was considered for regeneration analysis.

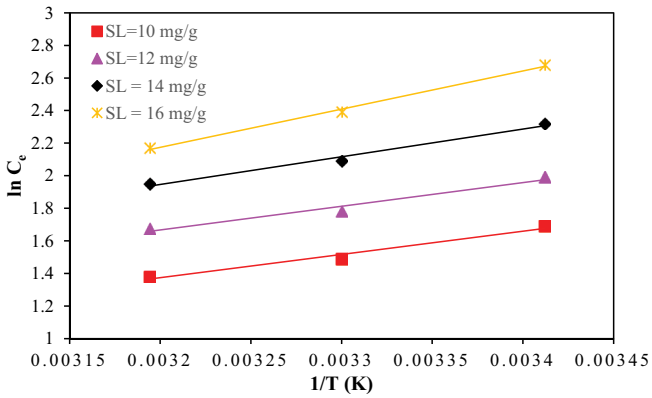

Fig. 9. Relation between $\ln(C_e)$ vs. $1/T$ for Malachite green adsorption onto MCGT-AC.

3.14. Analysis of chemical oxygen demand

For the analysis of chemical oxygen demand (COD), COD digester system was turned on and a temperature of 150°C was set. Such 10 digester tubes were considered and each of the tubes were fed with 50 mL of sample with MG dye concentration of 50 mg/L. They were added with mercuric sulphate and standard $K_2CR_2O_7$ (potassium dichromate, strength 0.125 N). After that, the tubes were placed in a plastic tray and allowed to cool before being filled with 50 mL of sulphuric acid reagent. The sulfuric acid reagent was slowly introduced. The solution was then thoroughly blended. The tubes were stored in a COD digester after the material was mixed. The air condensers were placed into the tubes, and the reflux of the mixture was set for 90 min. The air condensers were then removed from the tubes, as well

Table 8
MCGT-AC recycle-regeneration data using 1.0 M NaOH

No. of cycles	Residual concentration (mg/L)	Malachite green removal (%)
1st	0.12	95.7
2nd	0.79	88.2
3rd	1.77	79.5
4th	2.89	69.9
5th	3.34	60.3
6th	4.67	48.6

Table 9
Adsorption capacity and % adsorption by using different conc. of NaOH and HCl for MCGT-AC regeneration

Eluent	Concentration (M)	C_e (mg/L)	% Adsorption	q_e (mg/g)
HCl	0.2	4.67	48.3	1.21
	0.4	4.12	55.2	1.68
	0.6	3.34	69.5	1.43
	0.8	2.56	71.6	1.95
	1.0	1.45	80.4	1.78
NaOH	0.2	3.49	63.3	1.89
	0.4	3.12	69.5	1.37
	0.6	2.54	73.6	1.58
	0.8	1.68	79.4	2.85
	1.0	0.75	95.7	2.47

as the tubes from the COD digester, and the COD digester was allowed to cool to room temperature. Titration against 0.1 M ferrous ammonium sulphate solution with 1–2 drops of Ferroin indicator was used to measure the COD value (Assam State Pollution Control Board Manual). The test was conducted using a COD block digesting system (Model Pelican Kelplus-08L CAC). The COD value (in mg/L) was determined as follows:

$$\mathrm{COD}\left(\text{in}\frac{\text{mg}}{\text{L}}\right)=\frac{\left(\text{blank}-\text{sample}\right)\times 0.1\times 8000}{\text{volume of sample}} \tag{32}$$

Observations (not mentioned) revealed that before adsorption, COD value of sample solution was at 143.48 mg/L and the same has reduced to 44.67 mg/L after adsorption. Hence it is conclusive that, before adsorption due to presence of higher initial concentrations of MG dye, the COD value of the water solution was higher and as the solution was subjected to adsorption, dye concentration of the solution reduced and eventually the COD value of the solution came down. It also indicates that due to addition of MCGT-AC in the solution any increase in the COD value of the solution was insignificant, hinting that MCGT-AC was stable in water solution and was not releasing any chemical into the solution. The reduced COD value of the solution after the adsorption process and the removal of dye indicates the fitness of the MCGT-AC as an efficient adsorbent for the removal of MG dye from modelled dye solution.

3.15. Adsorption of MG onto MCGT-AC using real water samples

Table 10 shows the MG adsorption rate onto MCGT-AC using three distinct actual samples of water: wastewater, water from daily used tap and raw water. Faucets of laboratory were considered for collecting tap water, water from Gaurang River in Kokrajhar, Assam, India was considered as raw water and the wastewater sample was taken from an unnamed drain on the CITK campus. In 100.0 mL water samples, a specified quantity of MG dye was added to produce concentrations of 25, 50 and 75 mg/L. Experiments were conducted for 30 min and with a solution pH of 6.5. For reference, distilled water sample was used. According to the results, in comparison to modelling dye wastewater, the adsorption rate of MG by MCGT-AC in actual water samples was marginally enhanced.

Table 10
Malachite green adsorption onto MCGT-AC in real water samples

Water sample	Malachite green concentration (mg/L)	Malachite green removal (%)
Tap water	25	95.7
	50	80.5
	75	53.8
Raw water	25	95.6
	50	80.4
	75	54.9
Distilled water	25	95.4
	50	78.8
	75	54.3
Wastewater	25	94.6
	50	82.3
	75	54.7

4. Conclusion

Water hyacinth-derived activated carbon (AC) is effectively carboxylated with the help of sodium hydroxide, an organochlorine chemical, and mechanical attrition. The ability to adsorb substances is significantly influenced by changes in temperature, initial dye content, sorbent dose, pH, and interaction duration. Due to the addition of carboxyl, hydroxyl, and other active functional groups on the AC after surface alteration, MCGT-AC exhibits high adsorptive elimination of dye. The carboxylic group treatment of the activated carbon can also be credited with the creation of carbonate groups on the MCGT-AC surface as well as the generation of other basic groups that are comparable to carbonates. Due to the group's strong affinity for acid conjugate bases, good dispersion properties, and high magnitude of hydrophobic functional group rate for comparable amount of adsorbent, carboxylic group modified AC was found to be beneficial in removing cationic dye. The sorption of MG onto sorbent was verified by analysis using BET, XRD, ESEM, XEDS, FTIR, and HR-TEM. The analysis of zeta potential and pH_{PZC} provided a good indication of the sample solution's favourable and steady pH. Analysis of the pH range (2–9) showed that the rate at which colour was removed by the sorbent grew as pH rose. A higher temperature was validated for the spectrum of MG removal using MCGT-AC. (298–318 K). The pseudo-second-order kinetic model demonstrated the greatest agreement with the experimental results for the rate of the adsorption reaction. Error analysis and data comparison with isotherm models indicated that the Langmuir equation provided acceptable fit. Thermodynamic analysis indicated that adsorption was endothermic, with chemisorption (E_a = 51.36 kJ/mol) being the main contributor. The column analysis that supported the Langmuir model research found the Thomas model to be appropriate. Thermodynamic and temperature studies agreed with isosteric heat analysis. According to research on the sorption of MG onto MCGT-AC, carboxylic groups added to the surface of activated carbon significantly improve its capacity for adsorption. In conclusion, it was determined that AC modification using the methods covered in this paper is a viable study option for cationic dye sorption and can be effectively used for dye treatment of effluents containing dye pollutants.

Funding

This research did not receive any specific grant from funding agencies in the public, commercial, or not-for-profit sectors.

Credit authorship contribution statement

Rumi Goswami: Experiments, Data collection, writing, preparation, editing the manuscript, Interpretation, writing

manuscript. Data curation, Reviewing, Amit Kumar Dey: Conceptualization, Methodology, Supervision.

Data availability statement

The data used to generate the results in the paper will be available upon request.

Declaration of competing interest

The authors declare that they have no known competing financial interests or personal relationships that could have appeared to influence the work reported in this paper.

Acknowledgements

Authors acknowledge the contribution made by Environmental Engineering Lab, Department of Civil Engineering, Central Institute of Technology Kokrajhar, India. Authors also would like to thank sophisticated analytical instrument facility, Bombay, IIT Bombay, India.

References

[1] R. Foroutan, S.J. Peighambardoust, H. Aghdasinia, R. Mohammadi, B. Ramavandi, Modification of bio-hydroxyapatite generated from waste poultry bone with MgO for purifying methyl violet-laden liquids, Environ. Sci. Pollut. Res., 27 (2020) 44218–44229.
[2] S.J. Peighambardoust, O. Aghamohammadi-Bavil, R. Foroutan, N. Arsalani, Removal of malachite green using carboxymethyl cellulose-g-polyacrylamide/montmorillonite nanocomposite hydrogel, Int. J. Biol. Macromol., 159 (2020) 1122–1131.
[3] C. Arora, P. Kumar, S. Soni, J. Mittal, A. Mittal, B. Singh, Efficient removal of malachite green dye from aqueous solution using *Curcuma caesia* based activated carbon, Desal. Water Treat., 195 (2020) 341–252.
[4] A.K. Dey, A. Dey, R. Goswami, Adsorption characteristics of methyl red dye by Na_2CO_3-treated jute fibre using multi-criteria decision making approach, Appl. Water Sci., 12 (2022) 179, doi: 10.1007/s13201-022-01700-9.
[5] E. Bulut, M. Ozacar, I.A. Sengil, Adsorption of malachite green onto bentonite: equilibrium and kinetic studies and process design, Microporous Mesoporous Mater., 115 (2008) 234–246.
[6] A. Mittal, L. Krishnan, V.K. Gupta, Removal and recovery of malachite green from wastewater using an agricultural waste material, de-oiled soya, Sep. Purif. Technol., 43 (2005) 125–133.
[7] R. Goswami, A.K. Dey, Cationic dye removal using surface treated activated carbon as an adsorbent, Environ. Sci. Water Res. Technol., 8 (2022) 2545–2566.
[8] Y.-H. Wu, K. Xue, Q.-L. Ma, T. Ma, Y.-L. Ma, Y.-G. Sun, W.-X. Ji, Removal of hazardous crystal violet dye by low-cost P-type zeolite/carbon composite obtained from in situ conversion of coal gasification fine slag, Microporous Mesoporous Mater., 312 (2021) 110742, doi: 10.1016/j.micromeso.2020.110742.
[9] V. Kumar, P. Saharan, A.K. Sharma, A. Umar, I. Kaushal, A. Mittal, Y. Al-Hadeethi, B. Rashad, Silver doped manganese oxide-carbon nanotube nanocomposite for enhanced dye-sequestration: isotherm studies and RSM modelling approach, Ceram. Int., 46 (2020) 10309–10319.
[10] R. Goswami, A.K. Dey, Synthesis and application of treated activated carbon for cationic dye removal from modelled aqueous solution, Arabian J. Chem., 15 (2022) 104290, doi: 10.1016/j.arabjc.2022.104290.
[11] S. Pashaei-Fakhri, S.J. Peighambardoust, R. Foroutan, N. Arsalani, B. Ramavandi, Crystal violet dye sorption over acrylamide/graphene oxide bonded sodium alginate nanocomposite hydrogel, Chemosphere, 270 (2021) 129419, doi: 10.1016/j.chemosphere.2020.129419.
[12] H. Mittal, A. Al Alili, P.P. Morajkar, S.M. Alhassan, Graphene oxide crosslinked hydrogel nanocomposites of xanthan gum for the adsorption of crystal violet dye, J. Mol. Liq., 323 (2021) 115034, doi: 10.1016/j.molliq.2020.115034.
[13] R. Goswami, A.K. Dey, Use of anionic surfactant-modified activated carbon for efficient adsorptive removal of crystal violet dye, Adsorpt. Sci. Technol., 2022 (2022) 2357242, doi: 10.1155/2022/2357242.
[14] Z. Esvandi, R. Foroutan, S.J. Peighambardoust, A. Akbari, B. Ramavandi, Uptake of anionic and cationic dyes from water using natural clay and clay/starch/$MnFe_2O_4$ magnetic nanocomposite, Surf. Interfaces, 21 (2020) 100754, doi: 10.1016/j.surfin.2020.100754.
[15] C. Bouchelta, M.S. Medjram, O. Bertrand, J.P. Bellat, Preparation and characterization of activated carbon from date stones by physical activation with steam, J. Anal. Appl. Pyrolysis, 82 (2008) 70–77.
[16] A.K. Dey, A. Dey, Selection of Optimal Processing Condition During Removal of Methylene Blue Dye Using Treated Betel Nut Fibre Implementing Desirability Based RSM Approach, P. Kayaroganam, Ed., Response Surface Methodology in Engineering Science, InTechOpen, 2020, doi: 10.5772/intechopen.98428.
[17] B.M. Thamer, H. El-Hamshary, S.S. Al-Deyab, M.H. El-Newehy, Functionalized electrospun carbon nanofibers for removal of cationic dye, Arabian J. Chem., 12 (2019) 747–759.
[18] M. Teng, J. Qiao, F. Li, P.K. Bera, Electrospun mesoporous carbon nanofibers produced from phenolic resin and their use in the adsorption of large dye molecules, Carbon, 50 (2012) 2877–2886.
[19] A.K. Dey, A. Dey, R. Goswami, Fixed-bed column analysis for adsorption of Acid scarlet 3R dye from aqueous solution onto chemically modified betel nut husk fibre, Desal. Water Treat., 252 (2022) 381–390.
[20] Md. Munjur Hasan, M.A. Shenashen, Md. Nazmul Hasan, H. Znad, Md. Shad Salman, Md. Rabiul Awual, Natural biodegradable polymeric bioadsorbents for efficient cationic dye encapsulation from wastewater, J. Mol. Liq., 323 (2021) 114587, doi: 10.1016/j.molliq.2020.114587.
[21] A.R. Bagheri, M. Ghaedi, A. Asfaram, A.A. Bazrafshan, R. Jannesar, Comparative study on ultrasonic assisted adsorption of dyes from single system onto Fe_3O_4 magnetite nanoparticles loaded on activated carbon: experimental design methodology, Ultrason. Sonochem., 34 (2017) 294–304.
[22] A.K. Dey, A. Dey, Selection of optimal processing condition during removal of Reactive Red 195 by NaOH treated jute fibre using adsorption, Groundwater Sustainable Dev., 12 (2021) 100522, doi: 10.1016/j.gsd.2020.100522.
[23] M.Sh. Gohr, A.I. Abd-Elhamid, A.A. El-Shanshory, H.M.A. Soliman, Adsorption of cationic dyes onto chemically modified activated carbon: kinetics and thermodynamic study, J. Mol. Liq., 346 (2022) 118227, doi: 10.1016/j.molliq.2021.118227.
[24] N.P. Carnaje, R.B. Talagon, J.P. Peralta, K. Shah, J. Paz-Ferreiro, Development and characterisation of charcoal briquettes from water hyacinth (*Eichhornia crassipes*)-molasses blend, PLoS One, 13 (2018) e0207135, doi: 10.1371/journal.pone.0207135.
[25] W. Maulina, R. Kusumaningtyas, Z. Rachmawati, Supriyadi, A. Arkundato, L. Rohman, E. Purwandari, Carbonization process of water hyacinth as an alternative renewable energy material for biomass cook stoves applications, IOP Conf. Ser.: Earth Environ. Sci., 239 (2019) 012035, doi: 10.1088/1755-1315/239/1/012035.
[26] A.I. Abd-Elhamid, A.S. Doma, A.M. El-Syed, E.-R. Kenawy, Eco-friendly activation of charcoal for purification of water from colored organic pollutants, Res. J. Chem. Environ., 23 (2019) 83–95.
[27] A.K. Dey, U. Kumar, A. Dey, Use of response surface methodology for the optimization of process parameters for the removal of Congo red by NaOH treated jute fibre, Desal. Water Treat., 115 (2018) 300–314.

[28] ISO 13099-2 I. Colloidal Systems — Methods for Zeta-potential Determination — Part 2: Optical Methods, International Organization of Standards, Geneva, Switzerland, 2012.
[29] A. Dhillon, D. Kumar, Development of a nanoporous adsorbent for the removal of health-hazardous fluoride ions from aqueous systems, J. Mater. Chem. A, 3 (2015) 4215–4228.
[30] P.M. Thabede, N.D. Shooto, E.B. Naidoo, Removal of methylene blue dye and lead ions from aqueous solution using activated carbon from black cumin seeds, S. Afr. J. Chem. Eng., 33 (2020) 39–50.
[31] A.K. Dey, U. Kumar, Adsorption of anionic azo dye Congo red from aqueous solution onto NaOH-modified jute fibre, Desal. Water Treat., 92 (2017) 301–308.
[32] Z. Eren, F.N. Acar, Adsorption of Reactive Black 5 from an aqueous solution: equilibrium and kinetic studies, Desalination, 194 (2006) 1–10.
[33] W. Plazinski, W. Rudzinski, A. Plazinska, Theoretical models of sorption kinetics including a surface reaction mechanism: a review, Adv. Colloid Interface Sci., 152 (2009) 2–13.
[34] S.J. Peighambardoust, O. Aghamohammadi-Bavil, R. Foroutan, N. Arsalani, Removal of malachite green using carboxymethyl cellulose-g-polyacrylamide/montmorillonite nanocomposite hydrogel, Int. J. Biol. Macromol., 159 (2020) 1122–1131.
[35] A.K. Dey, A. Dey, R. Goswami, Selection of optimal performance characteristics during adsorption of Methyl red dye using sodium carbonate treated jute fibre, Desal. Water Treat., 260 (2022) 187–202.
[36] R.M. de Souza, H.B. Quesada, L.F. Cusioli, M.R. Fagundes-Klen, R. Bergamasco, Adsorption of non-steroidal anti-inflammatory drug (NSAID) by agro-industrial by-product with chemical and thermal modification: adsorption studies and mechanism, Ind. Crops Prod., 161 (2021) 113200, doi: 10.1016/j.indcrop.2020.113200.
[37] A.P. Nazar de Souza, Y.E. Licea, M.V. Colaço, J.D. Senra, N.M.F. Carvalho, Green iron oxides/amino-functionalized MCM-41 composites as adsorbent for anionic azo dye: kinetic and isotherm studies, J. Environ. Chem. Eng., 9 (2021) 105062, doi: 10.1016/j.jece.2021.105062.
[38] R. Foroutan, R. Mohammadi, S. Farjadfard, H. Esmaeili, B. Ramavandi, G.A. Sorial, Eggshell nano-particle potential for methyl violet and mercury ion removal: Surface study and field application, Adv. Powder Technol., 30 (2019) 2188–2199.
[39] A.K. Dey, U. Kumar, Adsorption of Reactive Red 195 from polluted water upon Na_2CO_3 modified jute fibre, Int. J. Eng. Technol., 9 (2017) 53–58.
[40] M.F.M. Yusop, M.A. Ahmad, N.A. Rosli, M.E. Abd Manaf, Adsorption of cationic methylene blue dye using microwave-assisted activated carbon derived from acacia wood: optimization and batch studies, Arabian J. Chem., 14 (2021) 103122, doi: 10.1016/j.arabjc.2021.103122.
[41] M. Feng, S. Yu, P. Wu, Z. Wang, S. Liu, J. Fu, Rapid, high-efficient and selective removal of cationic dyes from wastewater using hollow polydopamine microcapsules: isotherm, kinetics, thermodynamics and mechanism, Appl. Surf. Sci., 542 (2021) 148633, doi: 10.1016/j.apsusc.2020.148633.
[42] K. Sukla Baidya, U. Kumar, Adsorption of brilliant green dye from aqueous solution onto chemically modified areca nut husk, S. Afr. J. Chem. Eng., 35 (2021) 33–43.
[43] R. Goswami, A.K. Dey, Activated carbon from agricultural residues: a review, Desal. Water Treat., 278 (2022) 283–292.
[44] Á. Kuki, L. Nagy, M. Zsuga, S. Kéki, Fast identification of phthalic acid esters in poly (vinyl chloride) samples by direct analysis in real time (DART) tandem mass spectrometry, Int. J. Mass Spectrom., 303 (2011) 225–228.
[45] Z. Eren, F.N. Acar, Adsorption of Reactive Black 5 from an aqueous solution: equilibrium and kinetic studies, Desalination, 194 (2006) 1–10.
[46] M.E. Mahmoud, G.M. Nabil, N.M. El-Mallah, H.I. Bassiouny, S. Kumar, T.M. Abdel-Fattah, Kinetics, isotherm and thermodynamic studies of the adsorption of Reactive red 195 A dye from water by modified switchgrass biochar adsorbent, J. Ind. Eng. Chem., 37 (2016) 156–167.
[47] H.K. Mahilary, A.K. Dey, Preparation and application of carboxylated and mechanically attrited carbon for adsorptive removal of crystal violet dye, Environ. Sci. Water Res. Technol., 9 (2023) 861–882.
[48] C. Namasivayam, M.V. Suresh Kumar, Removal of chromium(VI) from water and wastewater using surfactant modified coconut coir pith as a biosorbent, Bioresour. Technol., 99 (2008) 2218–2225.
[49] D.H. Lataye, I.M. Mishra, I.D. Mall, Adsorption of α-picoline on granular activated carbon and rice husk ash from aqueous solution: Equilibrium and thermodynamic study, Chem. Eng. J., 147 (2009) 139–149.
[50] D.H. Lataye, I.M. Mishra, I.D. Mall, Removal of 4-picoline from aqueous solution by adsorption onto bagasse fly ash and rice husk ash: equilibrium, thermodynamic, and desorption study, J. Environ. Eng., 137 (2011) 1048–1057.
[51] Y. Yao, F. Xu, M. Chen, Z. Xu, Z. Zhu, Adsorption behaviour of methylene blue on carbon nanotubes, Bioresour. Technol., 101 (2010) 3040–3046.
[52] S. Sahu, S. Pahi, S. Tripathy, S.K. Singh, A. Behera, U.K. Sahu, R.K. Patel, Adsorption of methylene blue on chemically modified lychee seed biochar: dynamic, equilibrium, and thermodynamic study, J. Mol. Liq., 315 (2020) 113743, doi: 10.1016/j.molliq.2020.113743.
[53] N.S. Al-Kadhi, The kinetic and thermodynamic study of the adsorption Lissamine Green B dye by micro-particle of wild plants from aqueous solutions, Egypt. J. Aquat. Res., 45 (2019) 231–238.
[54] Z. Dehghani, M. Sedghi-Asl, M. Ghaedi, M.M. Sabzehmeidani, E. Adhami, Ultrasound-assisted adsorption of paraquat herbicide from aqueous solution by graphene oxide/mesoporous silica, J. Environ. Chem. Eng., 9 (2021) 105043, doi: 10.1016/j.jece.2021.105043.
[55] V. Gopal, K.P. Elango, Studies on defluoridation of water using magnesium titanate, Ind. J. Chem. Technol., 17 (2010) 28–33.
[56] M. Sarkar, A. Banerjee, P.P. Pramanick, A.R. Sarkar, Use of laterite for the removal of fluoride from contaminated drinking water, J. Colloid Interface Sci., 302 (2006) 432–441.
[57] K.Z. Elwakeel, A.A. El-Bindary, A.Z. El-Sonbati, A.R. Hawas, Magnetic alginate beads with high basic dye removal potential and excellent regeneration ability, Can. J. Chem., 95 (2017) 807–815.